INTERFACE

rsif.royalsocietypublishing.org

Research

Cite this article: Tagliazucchi E, Chialvo DR, Siniatchkin M, Amico E, Brichant J-F, Bonhomme V, Noirhomme Q, Laufs H, Laureys S. 2016 Large-scale signatures of unconsciousness are consistent with a departure from critical dynamics. *J. R. Soc. Interface* **13**: 20151027.
http://dx.doi.org/10.1098/rsif.2015.1027

Received: 28 November 2015
Accepted: 4 January 2016

Subject Areas:
biocomplexity, biophysics, medical physics

Keywords:
consciousness, anaesthesia, complex systems, phase transitions, fMRI

Author for correspondence:
Enzo Tagliazucchi
e-mail: tagliazucchi.enzo@googlemail.com

†These authors contributed equally to this work.

Electronic supplementary material is available at http://dx.doi.org/10.1098/rsif.2015.1027 or via http://rsif.royalsocietypublishing.org.

THE ROYAL SOCIETY PUBLISHING

Large-scale signatures of unconsciousness are consistent with a departure from critical dynamics

Enzo Tagliazucchi[1,2,†], Dante R. Chialvo[3,†], Michael Siniatchkin[1], Enrico Amico[4], Jean-Francois Brichant[4], Vincent Bonhomme[4], Quentin Noirhomme[4], Helmut Laufs[2,5,†] and Steven Laureys[4,†]

[1]Institute for Medical Psychology, Christian Albrechts University Kiel, 24105 Kiel, Germany
[2]Department of Neurology and Brain Imaging Center, Goethe University Frankfurt am Main, Frankfurt am Main, 60528 Frankfurt am Main, Germany
[3]Comision Nacional de Investigaciones Cientificas y Tecnologicas (CONICET), Buenos Aires, Argentina
[4]Coma Science Group, GIGA Research and Cyclotron Research Center, University and University Hospital of Liège, Liège, Belgium
[5]Department of Neurology, Christian Albrechts University Kiel, 24104 Kiel, Germany

Loss of cortical integration and changes in the dynamics of electrophysiological brain signals characterize the transition from wakefulness towards unconsciousness. In this study, we arrive at a basic model explaining these observations based on the theory of phase transitions in complex systems. We studied the link between spatial and temporal correlations of large-scale brain activity recorded with functional magnetic resonance imaging during wakefulness, propofol-induced sedation and loss of consciousness and during the subsequent recovery. We observed that during unconsciousness activity in frontothalamic regions exhibited a reduction of long-range temporal correlations and a departure of functional connectivity from anatomical constraints. A model of a system exhibiting a phase transition reproduced our findings, as well as the diminished sensitivity of the cortex to external perturbations during unconsciousness. This framework unifies different observations about brain activity during unconsciousness and predicts that the principles we identified are universal and independent from its causes.

1. Introduction

Anaesthetic drugs transiently impair awareness and thus offer a unique opportunity to investigate the neural correlates of conscious wakefulness. In contrast to other reversible unconscious states (such as sleep), anaesthetics simultaneously reduce arousal and awareness and—except in the rare event of intraoperative awareness—result in a brain state incompatible with conscious content [1]. Studies of the transition from wakefulness to loss of consciousness induced by propofol (a presumed GABA agonist anaesthetic agent) consistently report decreased cortical integration [1–6] and changes in the dynamics of electrophysiological brain signals, such as delta (1–4 Hz) and gamma oscillations (30–70 Hz) [7,8]. Despite many experimental reports at different temporal and spatial scales, the precise mechanisms underlying propofol-induced unconsciousness remain poorly understood. The need for a mechanistic understanding of this phenomenon is non-trivial, because it could contribute to unravelling how consciousness is constructed and preserved by the brain.

During conscious wakefulness, the cortex spontaneously generates a flurry of ever changing activity [9–11]. In the temporal domain, this activity is characterized by long-range temporal correlations, meaning that signal fluctuations at the present time influence dynamics up to several minutes in the future [12,13]. Lacking any distinctive scale (scale-free), these temporal correlations can be characterized by the computation of scaling exponents, such as the Hurst exponent [14]. In the spatial domain, these fluctuations are coordinated across

networks of regions commonly coactivated during stimulation and cognitive performance, termed resting state networks (RSNs) [15,16]. While functional connectivity can transiently dissociate from interareal anatomical connections [17], brain activity correlations computed over extended periods of time seem to be partially explained by the underlying anatomy [18–21]. This suggests that spontaneous brain activity can be understood as an ever-transient (or metastable) exploration of the wide repertoire of paths offered by the underlying structural connectivity, the extent of such exploration potentially depending on the brain state, with variable repertoires corresponding to different degrees of awareness.

Here, we put forward an interpretation of propofol-induced loss of consciousness in analogy to the dynamics and connectivity of fluctuations seen on a diversity of complex systems exhibiting different phases. As a system explores the space of possible configurations, its spatio-temporal correlations behave in characteristic ways. In particular, the dynamical changes underlying different degrees of awareness could be analogous to the qualitative changes observed in the dynamics of complex systems when they move away from a phase transition [22]. Experimental evidence gathered from functional magnetic resonance imaging (fMRI) data supports the view that during conscious wakefulness the human brain operates near the critical point of such a transition [9,23]. A robust feature of the critical state is the phenomenon of *critical slowing down*, which is manifest as increased temporal autocorrelation (i.e. long-range temporal correlations) of fluctuations throughout the system [9,24,25]. Far from the critical transition, the variables describing the system are very stable. As a consequence, any perturbation from equilibrium is dissipated quickly (i.e. dynamics rapidly return to equilibrium). Conversely, near the transition the effects of any disturbance last longer, thus the dynamics *slow down*. Because far from the transition the system is stuck in a stable state, its dynamics cannot explore the wider repertoire allowed by structural constraints. The opposite occurs near the phase transition at which the system can switch between a large number of locally stable or metastable states [24], and fully explore its structural connectivity [26,27]. Thus, if unconsciousness results in a departure from critical dynamics, then we expect to see these two inter-related signatures: (i) loss of temporal correlations in brain activity time series and (ii) a less complete exploration of the activity patterns allowed by the underlying structural connectivity.

Previous experimental results are consistent with a loss of critical slowing down in large-scale brain activity during unconsciousness. For instance, magnetic and electric perturbation of the cortex during different states of consciousness elicits equally different responses: conscious wakefulness is characterized by prolonged and spatio-temporally correlated responses (disturbances last longer), whereas unconsciousness is characterized by a smaller repertoire of rapidly vanishing and spatially localized responses [28–31]. The response to endogenous fluctuations during deep sleep is also rapidly vanishing, resulting in the loss of temporal long-range correlations [14]. Finally, spontaneous electrophysiological activity recorded during unconsciousness presents increased stability [32]. A mechanistic account of the action of propofol on large-scale brain activity should provide a unified explanation for these seemingly different experimental results.

To propose such an explanation, we studied fMRI data acquired during wakefulness, propofol-induced sedation and loss of consciousness, as well as during the subsequent recovery of awareness. We evaluated the presence of two large-scale signatures of a departure from the critical point of a phase transition: loss of long-range temporal correlations and the uncoupling of functional and anatomical connectivity [26,27], measured using diffusion tensor imaging (DTI) and diffusion spectrum imaging (DSI). Finally, we developed a conceptual model presenting a phase transition to assist in the mechanistic interpretation of the experimental results.

2. Methods

2.1. Experimental design and participants

Participants were scanned with fMRI during wakefulness (W), propofol sedation (S), propofol-induced loss of consciousness (LOC) and finally during the recovery of wakefulness (R). Sedation corresponded to Ramsay level 3 [33]. Loss of consciousness corresponded to Ramsay levels 5–6 (subjects did not exhibit responses to verbal instructions). Recovery corresponded to Ramsay level 2.

Twenty healthy right-handed volunteers aged between 18 and 31 years (22.4 ± 2.4 years) were initially included in the study. Following Monti *et al.* [5], subjects with head displacements exceeding 3 mm during any of the four conditions were discarded from the analysis, resulting in a final set of 12 participants. For all conditions, the resulting average head movement amplitudes did not exceed 1 mm (wakefulness: 0.38 mm, sedation: 0.25 mm, loss of consciousness: 0.17, recovery: 0.36 mm). No significant effect of condition on head displacement was found ($F_{3,44} = 2.63$, $p = 0.062$). As noted by Monti *et al.*, this is a conservative approach to limit the impact of head movement. Other methods, such as scan nulling [34], could affect the estimation of blood oxygen level-dependent (BOLD) signal spectral power and long-range temporal correlations and therefore were not applied. As an additional control, the presence of significant residual correlations between absolute and relative head movement time series and voxel-wise BOLD time series was evaluated after data pre-processing, with no significant residual correlations being detected.

Details on fMRI, DTI and DSI data acquisition and pre-processing are provided in the electronic supplementary material, Methods.

2.2. Estimation of long-range temporal dependencies

DFA [35] was applied to study the temporal correlations of BOLD fluctuations. This method was developed to obtain estimates of long-range temporal dependence in time series, while accounting for the possibility of non-stationarities. In the electronic supplementary material, Methods, we provide a formal definition of the procedure followed in the DFA algorithm. Briefly, time series were first de-trended by subtracting the mean, and the cumulative sum was then computed. Afterwards, the signal was divided into non-overlapping windows, and the intensity of the fluctuations was computed by averaging the standard deviation of the signal across all windows (de-trended within each window). This procedure was repeated for different window sizes, and the slope of the standard deviation of the fluctuations versus the window size ('fluctuation function', in logarithmic scale) was identified with the Hurst exponent (H). Based on the value of H, three qualitatively different scenarios can be distinguished: long-range temporal correlations (slow decay of the autocorrelation function) with $0.5 < H < 1$, uncorrelated temporal activity (exponential decay of the autocorrelation function) with $H = 0.5$ and long-range anti-correlations (switching between high and low values in consecutive time steps) with $0 < H < 0.5$.

We applied DFA to the first 150 volumes of the BOLD time series of every voxel for each subject and condition, obtaining spatial maps of H-values. To compute H, windows of length 10, 15, 25 and 30 volumes were used, as the logarithmic plot of the fluctuation function showed linear behaviour within this range. We also estimated H in the frequency domain following a wavelet-based method. The steps followed for the wavelet estimation of H are extensively presented and discussed in the electronic supplementary material, Methods.

2.3. Functional network construction

We constructed functional networks by extracting average BOLD signals from all regions of interest and computing the linear correlation between all pairs of signals, resulting in the correlation matrix C_{ij}.

For comparison with the underlying anatomical connectivity networks, the correlation matrices C_{ij} were thresholded to yield binary adjacency matrices A_{ij} such that $A_{ij} = 1$ if $C_{ij} \geq \rho$ and $A_{ij} = 0$ otherwise. The parameter ρ was chosen to fix the ratio of the connections in the network ($\Sigma_{i>j} A_{ij}$) to the total possible number of connections (termed link density). It is important to fix the link density when comparing networks, as otherwise differences could arise because the means of the respective C_{ij} are different (and therefore the number of non-zero entries in A_{ij}) and not because connections are topologically reorganized across conditions.

We performed all analyses for a range of link densities between 0.01 and 0.3 in steps of 0.01. When comparing functional networks with their anatomical counterparts, the chosen link density ranges always included the link density of the DTI and DSI anatomical networks.

2.4. Similarity between functional and anatomical connectivity neighbourhoods

We defined the connectivity neighbourhood of node i as $n_j = A_{ij}$ (i.e. the ith column of the adjacency matrix for a fixed local link density). According to this definition, the jth entry of n_j is 1 if nodes i and j share a direct connection in the network, and it is zero otherwise. We obtained the connectivity neighbourhood of all nodes in the anatomical and functional networks across all conditions and participants, as well as for a range of local link densities. To estimate the similarity between the anatomical and functional connectivity neighbourhoods of each node, we computed the Hamming distance between the anatomical and functional versions of vectors n_j (normalized by their total length). The Hamming distance is defined as the number of symbol substitutions (in this case 0 or 1) needed to transform one sequence into another and vice versa, and in this case, it is equal to twice the number of connections that must be re-wired to turn the functional connectivity neighbour into the anatomical connectivity neighbour.

2.5. Fluctuations in functional connectivity and repertoire of functional networks

We investigated if the fluctuations in the transient connectivity within the frontal executive control RSN were more widespread during wakefulness versus propofol-induced unconsciousness by computing the average functional connectivity of all nodes in the RSN over short non-overlapping windows of different durations. Afterwards, we computed the variance of the time series of dynamical functional connectivity fluctuations.

We investigated the repertoire of functional networks explored over time by means of a new methodology (see electronic supplementary material, figure S7 for a schematic). We first computed the connectivity matrices of all nodes within the executive control RSN (electronic supplementary material, figure S7*a*) over non-overlapping segments of 20 volumes. After thresholding at a given link density (ranging from 0.01 to 0.4), this defined a series of binary networks explored over time (electronic supplementary material, figure S7*b*). Afterwards, we computed the average correlation between the adjacency matrices of all these binary networks (electronic supplementary material, figure S7*c*). If the repertoire of explored networks is very constrained, then this average correlation is high (i.e. all transient networks are very similar). On the other hand, if the system explores a wide range of different transient networks, this average correlation is lower. We termed this index the transient network similarity (TNS) index.

2.6. Computational model

The computational model is based on the previous work of [36] (see also *a posteriori* similar formulation by Stam *et al*. [26]). It consists of an underlying anatomical network of connections (DSI network) and rules for the transition between three states: inactive, active and refractory. The rules for the transitions at the ith node are as follows

(1) inactive to active: either spontaneously with a probability of 10^{-3} or if $\Sigma_{j \text{ is active}} W_{ij} > T$;
(2) active to refractory always occurs and
(3) refractory to inactive with a probability of 10^{-1}.

These rules were used to simulate time series that were subsequently binarized by setting the active state to 1 and the other two to 0, and convolved with the standard haemodynamic response function mimicking brain neurometabolic coupling. As shown in [36], a second-order phase transition exists at $T_C \approx 0.05$. At this point, activity becomes self-sustained, spatial and temporal correlations are maximized, and an optimal agreement with the empirical fMRI data are obtained (including an approximate reproduction of the major RSN reported in the work of Beckmann *et al*. [15]).

3. Results

We first obtained the Hurst exponent and the low-frequency (0.01–0.1 Hz) power for each participant and condition (W, S, LOC and R). In addition, we investigated the same metrics in a phantom made of water (see electronic supplementary material, figure S1).

The anatomical distribution of Hurst exponent values and low-frequency power reflected the division of cortical anatomy into grey and white matter and cerebrospinal fluid. BOLD signals from grey matter voxels were characterized by long-range temporal correlations ($H > 0.65$), whereas white matter and cerebrospinal fluid voxels generally presented relatively weaker temporal correlations and 0.01–0.1 Hz frequency power (figure 1*a*). A shift towards reduced H and low-frequency power can be observed in the LOC condition (third row). We computed the global Hurst exponent and low-frequency power values (averaged across all grey matter voxels) and observed reduced values for the LOC condition relative to W (figure 1*b*). We also observed reduced values of the metrics in the frequency domain for R relative to W, suggesting that the recovery from propofol-induced loss of consciousness might not have been complete. Histograms for H and low-frequency power are shown in electronic supplementary material, figure S1. H-values peaked at around 0.5 (corresponding to temporally uncorrelated dynamics) for the water phantom and at $H > 0.5$ for grey matter brain

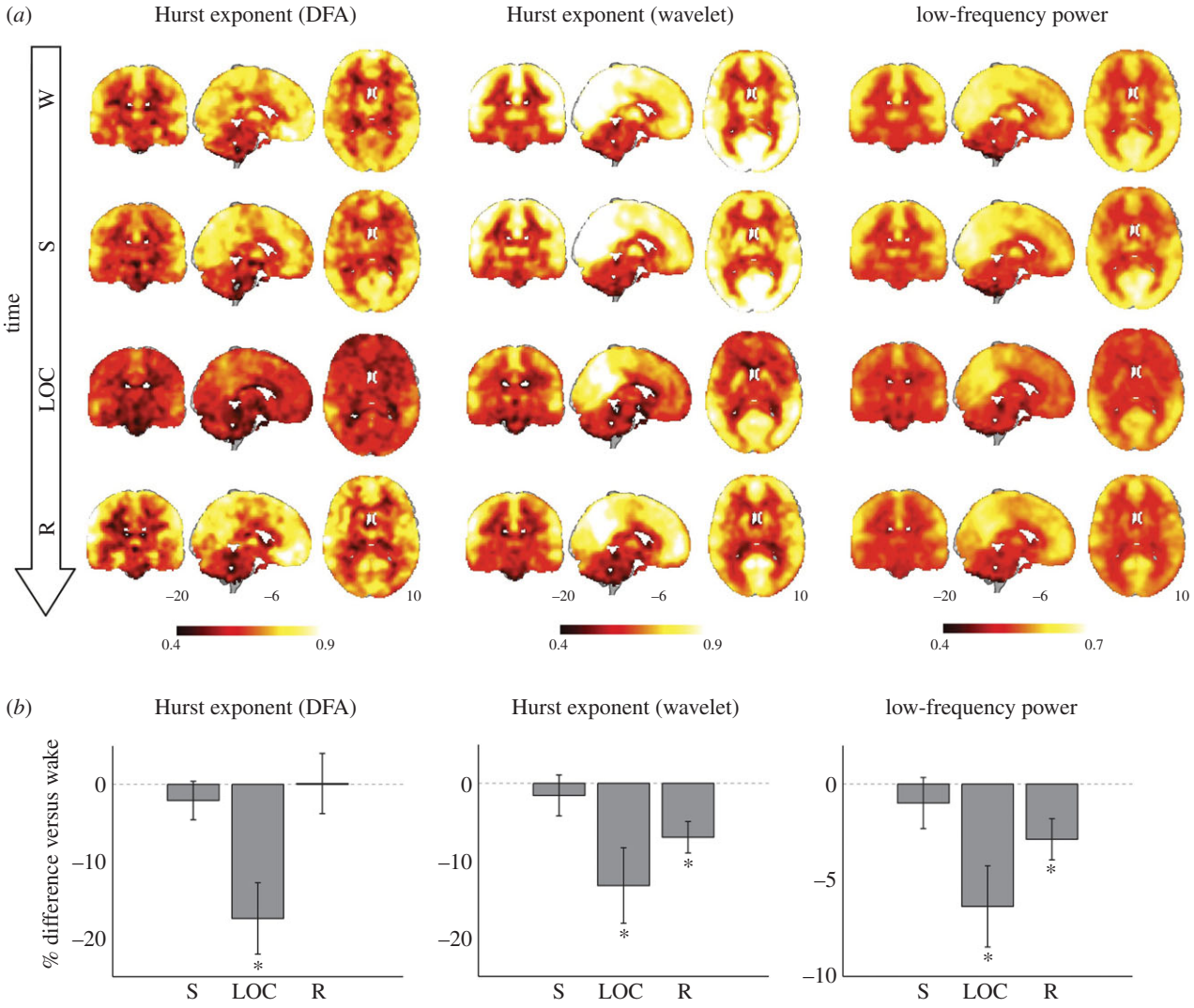

Figure 1. Anatomical specificity of long-range temporal correlations and low-frequency (0.01–0.1 Hz) fluctuations. (*a*) Anatomical overlays of the mean Hurst exponent (DFA and wavelet estimation) and low-frequency power for all experimental conditions; long-range temporal correlations and low-frequency fluctuations were predominantly observed in cortical and subcortical grey matter. (*b*) Differences in global Hurst exponents and low-frequency power relative to the values measured during wakefulness (*$p < 0.05$, Bonferroni corrected for multiple comparisons). (Online version in colour.)

voxels, i.e. as opposed to brain dynamics, those of the water phantom were temporally uncorrelated.

We conducted voxel-wise statistical tests to assess the effect of the condition on *H* and low-frequency power (figure 2). We observed a significant effect of the condition (W, S, LOC and R) on *H* (both DFA and wavelet-estimated) and 0.01–0.1 Hz power. This was observed in a set of regions comprising the thalamus, the ventromedial and orbitofrontal cortices, the frontal and rolandic operculi, the superior and medial frontal gyri and the anterior cingulate and bilateral insular cortices. Post hoc *t*-tests between W and all other conditions revealed significant decreases only for the comparison versus LOC. Similar results can also be observed in the first-order autoregressive coefficient of BOLD signals (electronic supplementary material, figure S2). Statistical parametric maps are presented in figure 2*a* (bottom panel). Figure 2*b* shows a ranking of the top 10 automated anatomical labelling (AAL) atlas [37] regions based on the statistical significance of the contrast W versus LOC. The extent of the overlap between the three different metrics is shown in figure 2*c* as a joint rendering of differences in H (both DFA and wavelet-estimated) and 0.01–0.1 Hz power. No significant differences were observed in terms of the goodness of fit (R^2) of the DFA fluctuation function. The covariance between the statistical significance maps derived from all three metrics is shown in electronic supplementary material, figure S3.

We then studied the coupling between anatomical and functional connectivity. At first, we restricted both functional and anatomical connectivity networks to a subnetwork encompassing the executive control network reported in reference [15], because this RSN overlapped with the regions where we found a breakdown of long-range temporal correlations during LOC (see electronic supplementary material, figure S4). For both DTI and DSI anatomical connectivity networks and almost all link densities, we observed decreased similarity between anatomical and functional connectivity networks during LOC relative to W (figure 3*a*).

Afterwards, we studied the local similarity between the anatomical and functional first neighbours of all individual nodes in whole-brain networks. The network nodes associated with decreased anatomical–functional coupling during LOC relative to W are shown in figure 3*b*. Differences encompassed the thalamus, as well as the medial prefrontal cortex, anterior cingulate cortex, frontal and rolandic operculi and the bilateral insular cortex. A ranking of AAL regions by their percentage of nodes with significant differences is presented in figure 3*c*. The

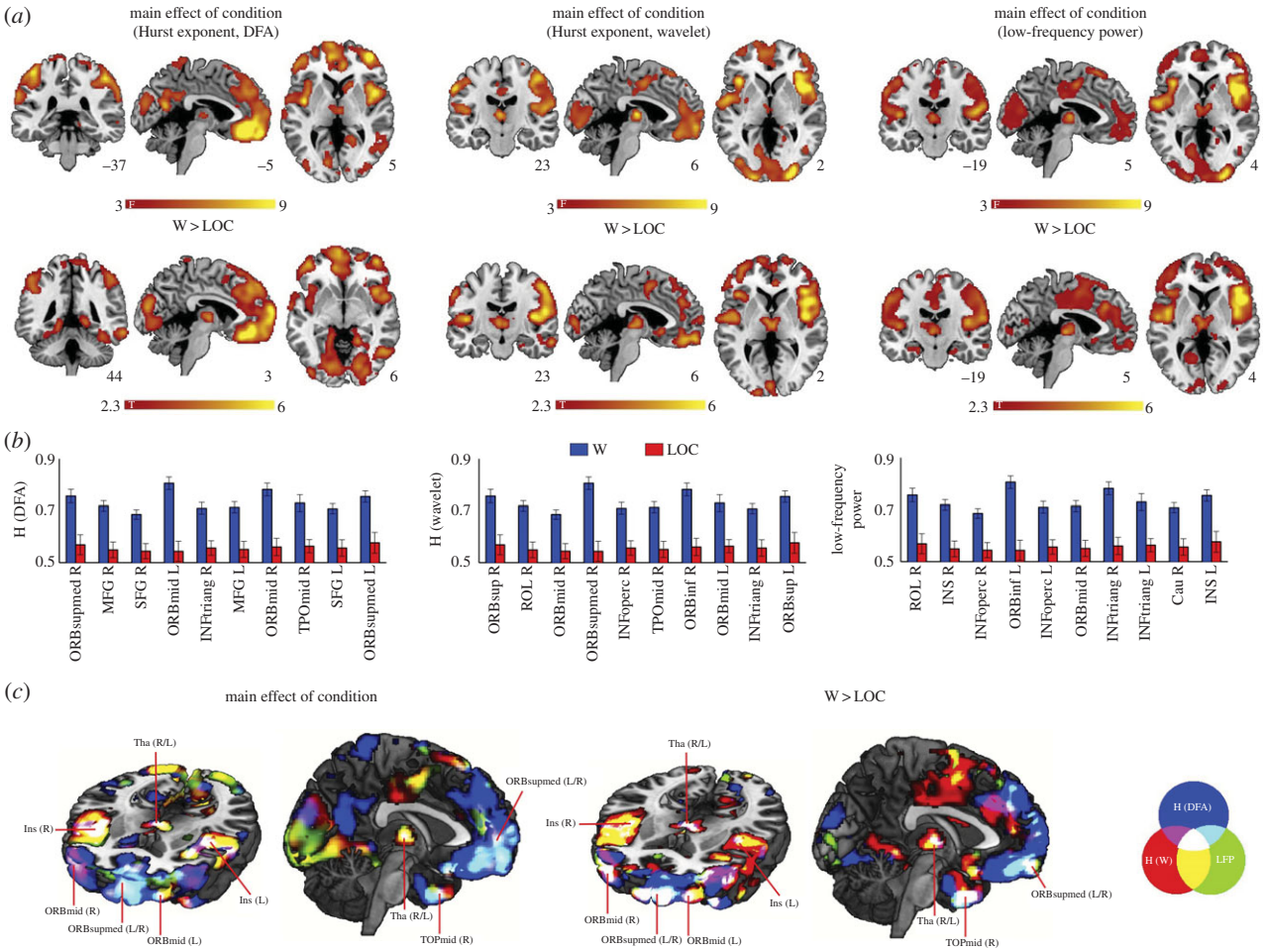

Figure 2. Breakdown of long-range temporal correlations and reduced low-frequency power fluctuations during propofol-induced loss of consciousness. (*a*) Top: main effect of experimental condition (wakefulness, sedation, loss of consciousness and recovery) on the Hurst exponent (DFA) and low-frequency power. Bottom: reduced Hurst exponent and low-frequency power during loss of consciousness compared with wakefulness. Both statistical significance maps were thresholded at $p < 0.05$, FDR-controlled for multiple comparisons. (*b*) Regions in the AAL atlas ranked according to their differences between wakefulness and loss of consciousness. (*c*) Combined anatomical overlay of the three metrics presented in (*a*). (Online version in colour.)

robustness of the results with respect to the two anatomical connectivity networks is manifest in the joint rendering of the nodes presenting significant differences (figure 3*d*). Similar results were obtained using partial correlations instead of linear correlations (see electronic supplementary material, figure S6).

As discussed in the Introduction, we hypothesized that during LOC the decorrelation of temporal dynamics should be seen together with a less thorough exploration of the repertoire of possible states allowed by anatomical constraints. To address this possibility, we investigated whether changes in H and low-frequency power during LOC were correlated with the degree of anatomy–function coupling. We computed the average anatomy–function Hamming distance within the significant regions in figure 3*b* (bottom panel) as a function of the link density, as well as the average H (DFA and wavelet-estimated) and 0.01–0.1 Hz frequency power in the same regions. This was performed for each participant in the LOC condition. We then computed the correlation coefficients and associated *p*-values between *H*, low-frequency power and the mean Hamming distance as a function of the link density. Results are shown in figure 4*a* (note that this correlation is against structural–functional network distance, not similarity). For both anatomical connectivity networks and almost all link densities, a significant negative correlation between *H* and the mean Hamming distance was found. Correlations involving low-frequency power were also negative but, in most cases, slightly above the threshold of statistical significance. Negative correlations imply that the stronger the decorrelation in temporal dynamics, the stronger the uncoupling between anatomical and functional connectivity. Figure 4*b* shows example scatterplots obtained at the reference link density of 0.15.

We then investigated the variability of functional connectivity over time to determine if unconsciousness was characterized by diminished fluctuations in dynamic connectivity, as predicted by a departure from criticality (see [36]). Results presented in figure 5*a* reveal that the variance of functional connectivity fluctuations (over a wide range of window sizes) was diminished during propofol-induced loss of consciousness. Furthermore, a wider range (repertoire) of functional networks was explored during conscious wakefulness compared with unconsciousness (figure 5*b*), as quantified by the TNS index computed using windows of 20 volumes.

To further gauge the significance of our observations, we introduced a simple dynamical model to evaluate which qualitative aspects of the propagation of information in anatomical networks were more relevant to replicate our empirical observations. The model allows three possible states for each node in the DSI network. The possible node states and transitions between them are illustrated in electronic supplementary material, figure S5.

The threshold in the model controls the propensity of excitations to propagate throughout the anatomical network.

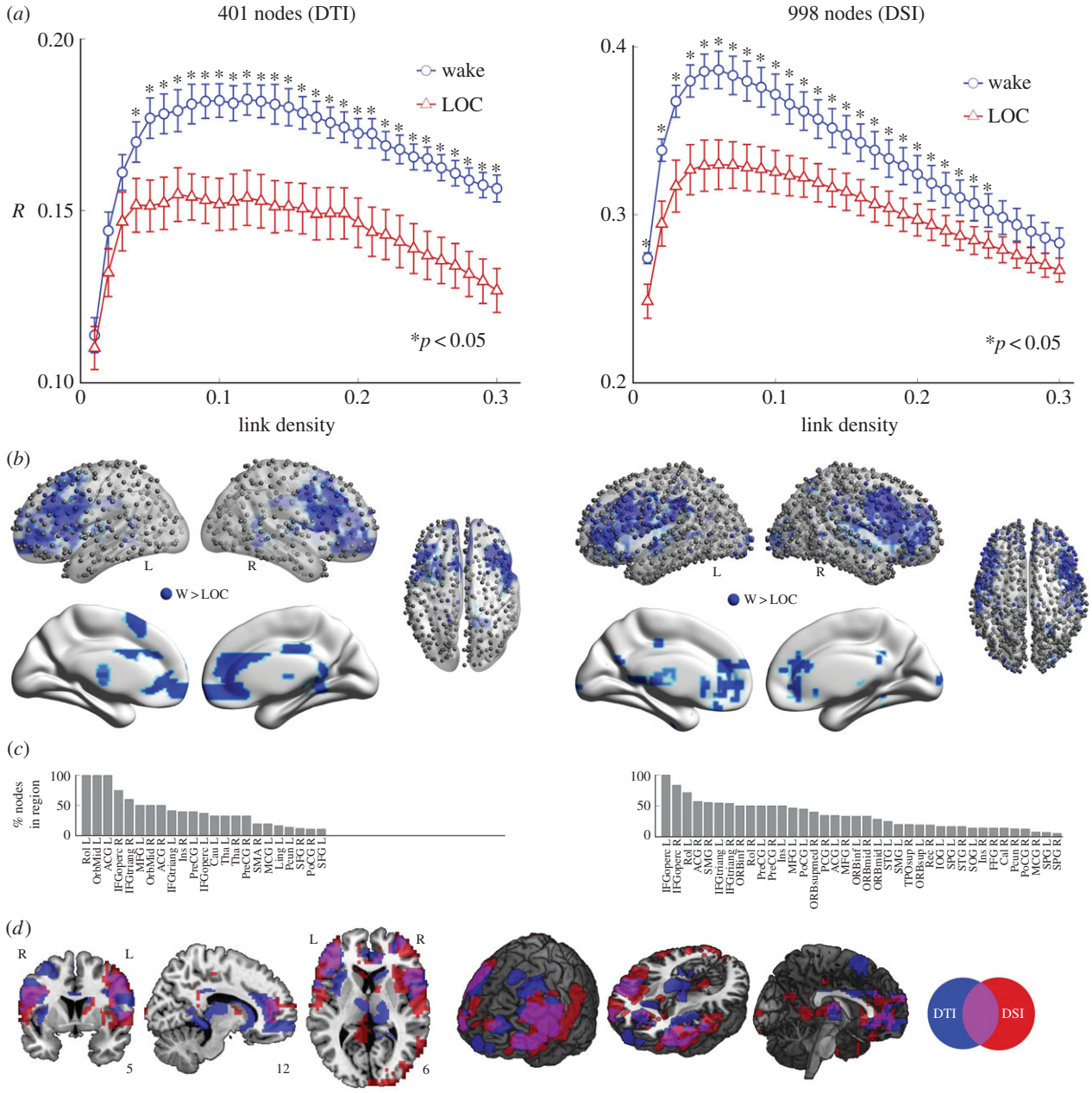

Figure 3. Regional dissociation of anatomical and functional connectivity during loss of consciousness. Results in the left column were obtained using the DTI network with 401 nodes, those in the right column using the DSI network with 998 nodes. (*a*) Similarity (correlation coefficient) between anatomical and functional connectivity networks within the executive control RSN as a function of link density, obtained during wakefulness (blue) and loss of consciousness (red). (*b*) Anatomical overlay of regions with significant increases in anatomical–functional distance during loss of consciousness versus wakefulness. (*c*) Ranking of AAL regions according to the percentage of nodes they contained with significant differences in anatomical–functional distance. (*d*) Joint anatomical rendering of results obtained using the DTI and DSI anatomical connectivity networks. (Online version in colour.)

Values higher than the critical threshold of $T_C \approx 0.05$ hinder the propagation of activity, which eventually dies out. On the other hand, lower thresholds result in self-sustained activity. Very low values result in the extreme of many nodes becoming rapidly activated and then transitioning towards the refractory ('hyperpolarized') state. A critical point exists at $T_C \approx 0.05$, marked by self-sustained activity allowing the reproduction of many features of large-scale brain activity, such as long-range temporal correlations in space and time and the emergence of coordinated structures strongly resembling RSN. The critical point corresponds to a second-order phase transition, characterized by maximal variability in the intrinsic dynamics of the system, critical slowing down and an optimal exploration of the repertoire of metastable state (i.e. states in which the system transiently resides). Examples of the temporal dynamics during the sub-, super- and critical regimes are shown in electronic supplementary material, figure S5.

We found that the similarity between functional and structural connectivity was maximal near the critical point. This was evident from computing the correlation between functional and anatomical adjacency matrices at each threshold value (figure 6*a*, left) or by computing the Hamming distance between the binarized functional and anatomical connectivities of each node (figure 6*a*, right). The frequency at which activations occurred correlated negatively with the threshold. As shown in figure 6*b* (left), low values facilitated the propagation of activity and induced higher activation rates, whereas higher thresholds caused the opposite effect by hindering the propagation of activity. In the supercritical ($T > T_C$) regime, the frequency of

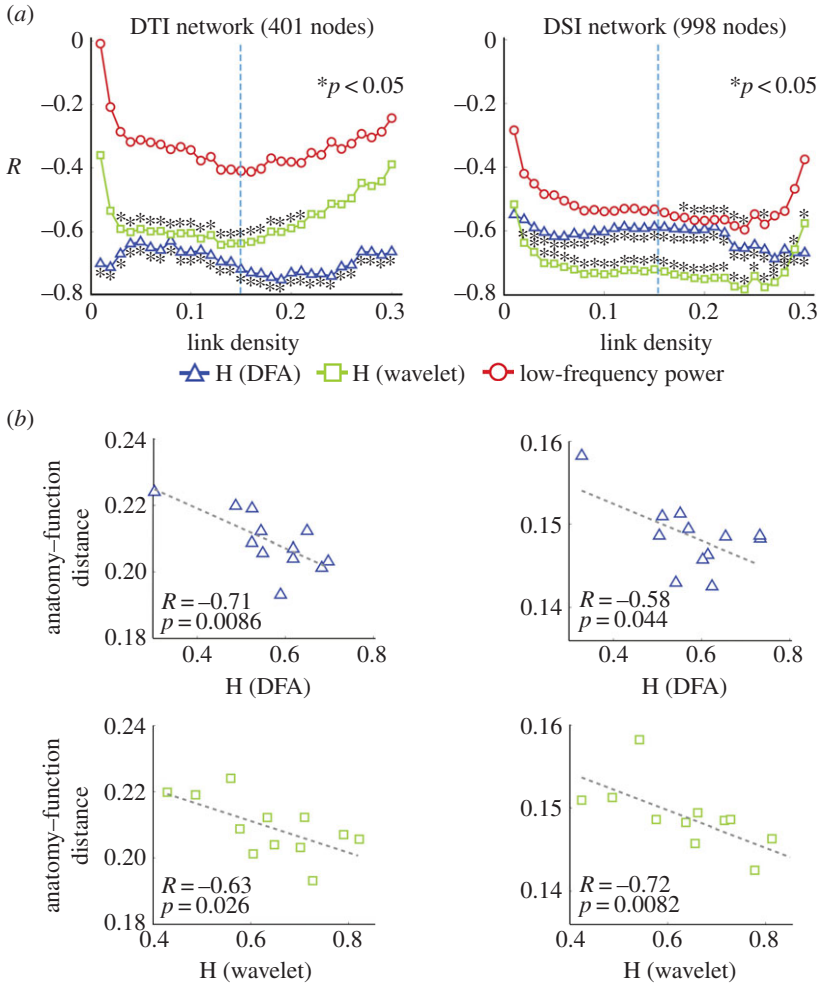

Figure 4. Changes in long-range temporal correlations and anatomical–functional coupling are correlated during loss of consciousness. (*a*) Left: correlation coefficient between the Hurst exponent (DFA and wavelet estimation) and low-frequency power averaged over the regions in figure 3*b*, and the average distance between anatomical (DTI) and functional connectivity; results are shown as a function of the link density. Right: same computation for the DSI network. (*b*) Scatter plots of anatomy–function distance versus H (DFA and wavelet estimation) for a reference link density of 0.15 (light blue dashed line in *a*). (Online version in colour.)

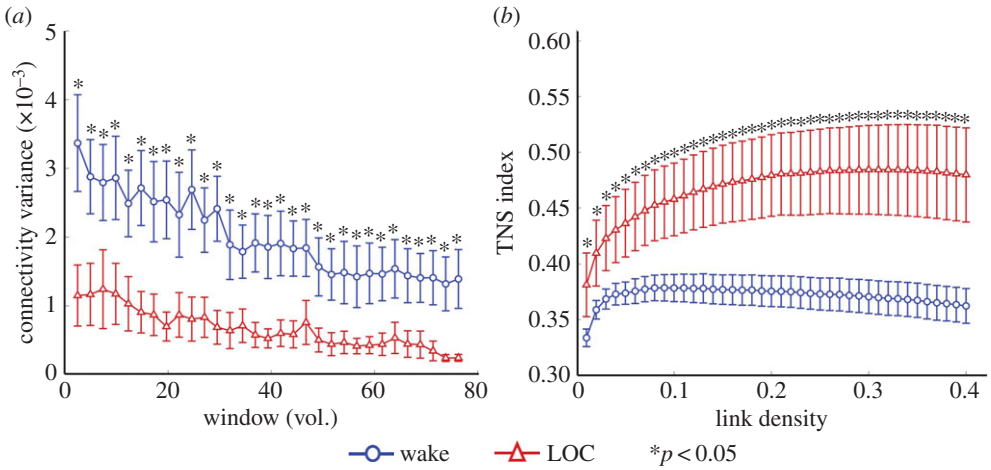

Figure 5. Unconsciousness increases network stability and decreases the repertoire of transient network states. (*a*) The variance of transient average connectivity within the executive control RSN as a function of non-overlapping window size, for wakefulness and loss of consciousness. (*b*) TNS index (computed using non-overlapping windows of 20 volumes) for wakefulness and loss of consciousness. (Online version in colour.)

activations also correlated negatively with the anatomical–functional distance (figure 6*b*, right). The same result was observed for the Hurst exponent of the average activity generated by the model. Both are consistent with the changes observed under propofol: the higher the uncoupling between anatomical and functional connectivity, the faster and less temporally correlated the dynamics of the system.

The critical slowing down observed when dynamics are close to the phase transition maximizes the response of the model to external perturbations. We studied the average response of the system to a sudden excitation of 60% of the nodes. This computation is of interest to evaluate which phases of the model better correspond to the diminished response to magnetic perturbations of cortical activity

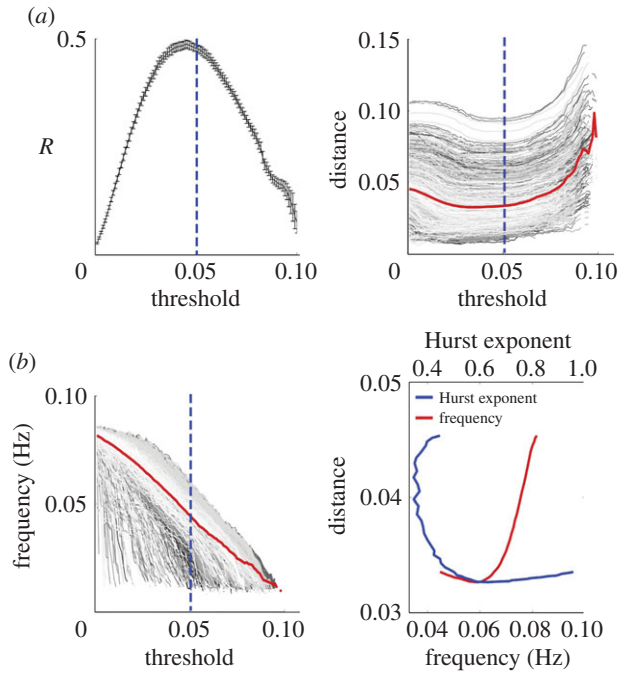

Figure 6. Dynamics and connectivity of the model. (*a*) Left: similarity between anatomical and functional (i.e. simulated) connectivity as a function of the threshold *T*. Right: Hamming distance between anatomical and functional node connectivity neighbourhoods (averaged across all nodes) as a function of *T*. In both cases, the highest anatomical–functional coupling is observed close to the critical point ($T = T_C$). (*b*) Left: frequency of node activations as a function of *T*. Right: mean anatomical–functional distance as a function of frequency of node activations and Hurst exponent of average activity of the model. As in the experimental data, higher frequency of activations and diminished long-range temporal correlations paralleled the dissociation between anatomical and functional connectivity patterns. (Online version in colour.)

observed during loss of consciousness. In figure 7 (left), we show the average time course after a perturbation (computed over 100 simulations) both for $T_C \approx 0.05$ and for $T_C < T = 0.01$. The response in the critical case was characterized by a sustained oscillation, with temporally persistent activity observed after the perturbation. On the other hand, the perturbation in the supercritical case induced a transient response rapidly giving way to a baseline of uncorrelated oscillations. We measured the decay of the variance in the activity over short temporal windows of 20 time steps. The activity decay after the perturbations is shown in figure 7 (centre) for all thresholds. By measuring the time elapsed until a level of low variance (10^{-5}) was crossed, we estimated the time necessary for the activity to decay to its baseline. The decay time peaked near the critical point and quickly decreased both in the super- and subcritical cases (figure 7, right).

4. Discussion

We studied how propofol-induced loss of consciousness affected the temporal dynamics of BOLD signals and how the changes in large-scale dynamics were related to the exploration of the underlying anatomical connectivity. Loss of consciousness was paralleled by a shift towards faster and temporally uncorrelated BOLD signals in the frontal lobe, the salience network and the thalamus. Within the same regions, functional connectivity departed from the underlying anatomical constraints; this departure covaried with loss of long-range temporal correlations.

An interpretation for our results is given in figure 8. We show a schematic depiction of an elementary system composed of interacting units, the state of the system being symbolized by the position of a particle within a potential landscape with several local equilibria (potential wells). In reality, this potential would span a high-dimensional space, with the state vector describing a multitude of independent variables characterizing the system at each time point. However, we adopt this simplified schematic for illustration purposes. Far from the critical point of a phase transition (left panel), the system is more stable, and the local minima are deeper; in consequence, any external perturbation or internal fluctuation rapidly vanishes and the particle returns quickly to the same local equilibrium. For the same reason, the dynamics of the system do not allow the exploration of all possibilities offered by the structural connectivity and thus functional correlations reflect only a portion of the anatomical connections. Near the phase transition (right panel), the landscape becomes shallower, the stability decreases and perturbations can induce a more widespread exploration of the potential landscape (see also figure 5), resulting in more sustained changes. As the system explores the neighbourhood of different local equilibria (or metastable states), spatial correlations better reproduce its structural connectivity. Our observations of large-scale fMRI dynamics and connectivity during loss of consciousness can be interpreted as a departure from a critical state (near the transition) towards more stable fluctuations (far from the transition).

Our model also allowed us to simulate the effect of perturbations near and far from its phase transition and thus to connect two robust but seemingly unrelated findings characterizing states of reduced awareness: loss of temporal complexity (i.e. long-range temporal correlations [14]) and rapidly vanishing responses to direct magnetic and electric stimulation of the cortex [28–30,38]. Within our framework, both arise as a result of increased stability, with endogenous as well as exogenous fluctuations failing to displace the system between different metastable states.

The mechanisms by which propofol could result in dynamics compatible with a departure from a phase transition deserve further investigation. Most likely, these consist of alterations in the properties of individual units (neurons or groups of neurons) translating into dramatically different collective behaviours. For instance, our model suggests that facilitated spreading of activity results in a state of global hyperpolarization (see electronic supplementary material, figure S5) impairing the propagation of external perturbations throughout the system. A possible correlate of this facilitated spreading is the increased power in the gamma frequency band observed during propofol-induced unconsciousness [7,8], which is also a main driver of BOLD activity fluctuations [39].

Contemporary theories postulate that consciousness is an emergent phenomenon of physical processes in the brain. The explanation of subjective experiences from the objective observation of these processes has remained elusive to neuroscience. However, it is possible to ask what features of brain activity are compatible with the rich subjective phenomenology of consciousness. An aspect common to different theories is that consciousness can be associated with a state of high *neural* complexity [40,41]. This can be understood as a state

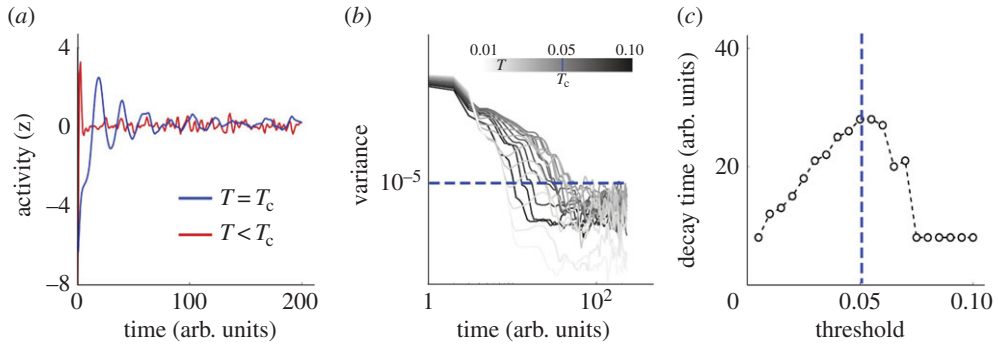

Figure 7. The sensitivity to external perturbations is maximal near the phase transition of the model. (*a*) Average time course after a perturbation (activation of 60% of the nodes) during the critical and supercritical regimes. (*b*) Decay of activity after a perturbation for a range of thresholds. (*c*) Decay time as a function of *T*. The longest decay times are obtained when $T = T_c$. (Online version in colour.)

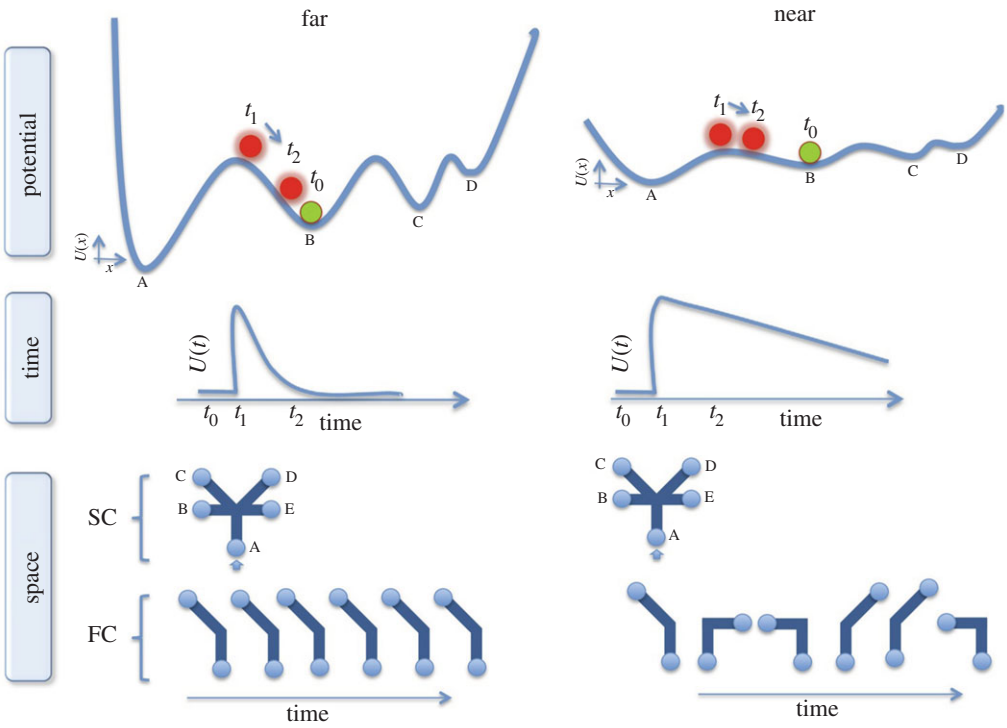

Figure 8. Schematic of the dynamics of a system far and near the critical point of a phase transition. The state of the system at a given time is represented by the position of the particle on the potential landscape $U(x)$. The system at equilibrium (green) is perturbed at t_0 subsequently relaxing (red, $t_1 \rightarrow t_2$) at different speeds depending on whether it is far (left) or near (right) a phase transition. Far from the transition (left), the system is stable and the local minima (equilibrium points) are deep, consequently dynamics are rapidly restored and the effects of perturbation are short-lasting. Near the phase transition (right), the landscape of the potential is shallow and consequently the stability of the local minima decreases, which is reflected in the time domain (middle panels) as a slowing down of the system response to fluctuations. The change in stability can be also observed spatially because it affects the exploration of the different metastable states of the system. The graphs denoted by structural connectivity (SC) represent a portion of the underlying structural network. The bottom diagram (functional connectivity, FC) denotes the structural paths traversed during an interval of time. For shallow local minima, the structural paths leading from node A to the rest of the nodes (B–E) are equally likely, resulting in a complete exploration of the underlying structural connectivity. On the contrary, far from the transition (left) the potential barriers separating the nodes are taller, leading to the observation of only a portion (in this case only one) of all possible paths. (Online version in colour.)

between the extremes of very high differentiation without information integration (the dynamics of each unit in the system become independent, like in a 'disordered' or 'random' system at the supercritical state) and very low differentiation (the system presents few possible states, as in an 'ordered' or 'regular' subcritical system). At the—between ordered and disordered—critical state, dynamics are both integrated (the units of the system present long-range correlations both in time and space) and segregated (the system allows the exploration of a large number of possible metastable states), suggesting this is the state that could maximize the standard definition of neural complexity. Future work will need to formally address a possible equivalence between metrics of *neural complexity* and metrics of criticality (i.e. order parameters).

Our research provides evidence that the 'baseline' state of wakeful rest presents critical dynamics and that unconscious brain states depart from this kind of dynamics. Thus, we identify critical dynamics with the state of consciousness. Because the possibility of having conscious, reportable content ('*I see X, hear Y, feel Z*') is in general conditional to being in a conscious state; critical dynamics could also be a necessary requirement for conscious content to emerge. This is supported by the observation of comparable neural complexity at rest and during conscious information access [42]. Furthermore, the role that critical dynamics play in

conscious information access could be related to the observation that at criticality the response of the system to external stimuli is maximized (figure 7). Because conscious perception requires the engagement of a distributed set of neurons (*dynamical core*; [41], as well as in the concept of the *global workspace*; [43]), a prerequisite is a high sensitivity to incoming stimuli (high *susceptibility*). Conversely, at the sub- or supercritical states, sensory stimulation results in a local and transient perturbation failing to propagate to more widespread networks related to conscious perception.

At other spatial and temporal scales, evidence for an association between consciousness and critical dynamics has been obtained in the context of deep sleep [44], anaesthesia [45,46] and epileptic seizures [47]. Here, we introduced the coupling between anatomical and functional connectivity as a signature of the critical state, which is particularly fit for fMRI recordings, because both can be measured at the same spatial resolution using this technique. Propofol-induced loss of consciousness resulted in diminished anatomical–functional coupling, interpreted here as a departure from the critical regime characteristic of conscious wakeful rest [23,48]. Changes in function–anatomy uncoupling can be understood in terms of the emergence of long-range correlations at criticality. The term 'long-range' must be treated with caution when discussing the human brain, because regions far away in Euclidean space may be close together in a topological sense (i.e. directly connected anatomically). Thus, we did not expect to see a breakdown of long-range functional connectivity as a function of Euclidean distance following the departure from criticality, but a separation from the structural connectivity backbone instead.

Recent work on anaesthetized primates [49] found that transient patterns of functional connectivity strongly resembling the anatomical constraints were more frequent during loss of consciousness relative to wakefulness, which appears to contradict our results. However, two important differences must be taken into account. First, we found diminished anatomy–function coupling over *extended* periods of time, which is related to the average of the functional connectivity states visited over time (as an analogy, mapping the average route traced by cars in a city throughout an entire day, as opposed to taking instantaneous snapshots). Second, the effect we report was regionally localized to a set of frontal regions and the thalamus, as opposed to the global effect reported in [49]. This last distinction is very important, because the richness of anatomical connectivity varies throughout the brain, from the regular structure of the cerebellum and primary cortices to the highly complex, variable and phylogenetically advanced frontal and parietal associative cortices [50,51]. Indeed, we observed that the functional exploration of frontothalamic anatomical connectivity was hindered under propofol, highlighting its importance for the maintenance of conscious awareness. We note that decreased similarity between anatomical and functional connectivity could also result from the selective enhancement of functional connections that are not associated with structural links (as an analogy, cars taking 'shortcuts' across regions not directly connected by roads). This possibility is ruled out by the breakdown of within- and between-network functional connectivity observed during propofol-induced unconsciousness [3].

We also studied the dynamics of BOLD signals, which have received comparatively less attention in the context of anaesthesia than electrophysiological recordings. We observed a departure from slow and temporally correlated dynamics in frontal regions and in the thalamus. These areas strongly overlap with those where decreased metabolism under anaesthesia was reported [52–55]. Breakdown of long-range temporal correlations was also reported in other unconscious brain states such as deep non-rapid eye movement sleep [14]. This led us to hypothesize that long-range temporal correlations of spontaneous activity fluctuations are a primary characteristic of brain activity during conscious wakeful rest. Phenomenologically, the subjective feeling of continuity during conscious wakefulness ('stream of consciousness', as famously phrased by James [56]), cannot be supported by short-range temporal correlations as exhibited, for example, in Markovian dynamics (when the state of the system depends only on the immediately previous state). The short-term persistence of conscious information is impossible under these dynamics unless structural changes occur, which likely belong to a completely different temporal scale [57].

The main limitation of our work arises from the indirect nature of fMRI recordings and the possibility of propofol influencing other physiological variables that are not directly related to the level of consciousness. Experimental evidence shows that the effects of propofol on arterial blood pressure and cerebral blood flow are small [58–61], ruling out confounding effects related to pressure-dependent changes in BOLD signals. As discussed by Hudetz *et al.* [62], confounding effects owing to alterations in neurovascular coupling are also unlikely given the preservation of functional responses during propofol-induced loss of consciousness [63]. Experiments measuring cardiac and respiration rates simultaneously with fMRI during propofol-induced loss of consciousness did not find a significant difference versus conscious wakefulness [64]. Another possibility is that our results reflect the concentration of propofol in blood but not the responsiveness of the participants [65]. One argument against our results reflecting the increasing concentration of propofol in blood is the fact that we did not observe any significant effects under propofol-induced sedation (a state characterized by responsiveness in spite of non-zero propofol plasma concentration). Our results were specific to unconsciousness, as determined by the onset of the state of unresponsiveness [33].

In summary, we achieved an empirical characterization of large-scale brain activity during propofol-induced unconsciousness in terms of inter-related changes in spatial and temporal correlations. In analogy to other complex systems undergoing phase transitions, the dynamics became temporally uncorrelated during unconsciousness and failed to efficiently explore the underlying structural connections. Because the proposed interpretation is based on general principles of complex systems, further research should reveal the universality of our findings across other brain states of diminished awareness, as well as investigate their applicability for the objective assessment of levels of consciousness.

Author contributions. E.T. and D.R.C. analysed data and wrote the paper; M.S., E.A. and H.L. edited the paper; J.F.B., V.B. and Q.N. contributed to data collection; S.L. designed the study, contributed to data collection and edited the paper.

Competing interests. We declare we have no competing interests.

Funding. This work was supported by the Bundesministerium für Bildung und Forschung (grant no. 01 EV 0703) and the LOEWE Neuronale Koordination Forschungsschwerpunkt Frankfurt (NeFF). E.T. is supported by an AXA Research Fund postdoctoral fellowship.

Acknowledgements. We thank Ben Palanca and two anonymous reviewers for valuable comments on this manuscript, Ed Bullmore and Nicolas Crossley for sharing the DTI data and Patric Hagmann and Olaf Sporns for sharing the DSI data.

References

1. Alkire MT, Hudetz AG, Tononi G. 2008 Consciousness and anesthesia. *Science* **322**, 876–880. (doi:10.1126/science.1149213)
2. Lee U, Mashour GA, Kim S, Noh GJ, Choi BM. 2009 Propofol induction reduces the capacity for neural information integration: implications for the mechanism of consciousness and general anesthesia. *Conscious. Cogn.* **18**, 56–64. (doi:10.1016/j.concog.2008.10.005)
3. Boveroux P *et al.* 2010 Breakdown of within- and between-network resting state functional magnetic resonance imaging connectivity during propofol-induced loss of consciousness. *Anesthesiology* **113**, 1038–1053. (doi:10.1097/ALN.0b013e3181f697f5)
4. Schrouff J *et al.* 2011 Brain functional integration decreases during propofol-induced loss of consciousness. *Neuroimage* **57**, 198–205. (doi:10.1016/j.neuroimage.2011.04.020)
5. Monti MM *et al.* 2013 Dynamic change of global and local information processing in propofol-induced loss and recovery of consciousness. *PLoS Comput. Biol.* **9**, e1003271. (doi:10.1371/journal.pcbi.1003271)
6. Amico E *et al.* 2014 Posterior cingulate cortex-related co-activation patterns: a resting state fMRI study in propofol-induced loss of consciousness. *PLoS ONE* **30**, e0100012. (doi:10.1371/journal.pone.0100012)
7. Murphy M *et al.* 2011 Propofol anesthesia and sleep: a high-density EEG study. *Sleep* **34**, 283.
8. Boly M *et al.* 2012 Connectivity changes underlying spectral EEG changes during propofol-induced loss of consciousness. *J. Neurosci.* **32**, 7082–7090. (doi:10.1523/JNEUROSCI.3769-11.2012)
9. Chialvo DR. 2010 Emergent complex neural dynamics. *Nat. Phys.* **6**, 744–750. (doi:10.1038/nphys1803)
10. Raichle ME. 2011 The restless brain. *Brain Connect.* **1**, 3–12. (doi:10.1089/brain.2011.0019)
11. Sporns O. 2011 The non-random brain: efficiency, economy, and complex dynamics. *Front. Comp. Neurosci.* **5**. (doi:10.3389/fncom.2011.00005)
12. Maxim V, Şendur L, Fadili J, Suckling J, Gould R, Howard R, Bullmore E. 2005 Fractional Gaussian noise, functional MRI and Alzheimer's disease. *Neuroimage* **25**, 141–158. (doi:10.1016/j.neuroimage.2004.10.044)
13. He BJ. 2011 Scale-free properties of the functional magnetic resonance imaging signal during rest and task. *J. Neurosci.* **31**, 13 786–13 795. (doi:10.1523/JNEUROSCI.2111-11.2011)
14. Tagliazucchi E, von Wegner F, Morzelewski A, Brodbeck V, Jahnke K, Laufs H. 2013 Breakdown of long-range temporal dependence in default mode and attention networks during deep sleep. *Proc. Natl Acad. Sci. USA* **110**, 15 419–15 424. (doi:10.1073/pnas.1312848110)
15. Beckmann CF, DeLuca M, Devlin JT, Smith SM. 2005 Investigations into resting-state connectivity using independent component analysis. *Phil. Trans. R. Soc. B* **360**, 1001–1013. (doi:10.1098/rstb.2005.1634)
16. Smith SM *et al.* 2009 Correspondence of the brain's functional architecture during activation and rest. *Proc. Natl Acad. Sci. USA* **106**, 13 040–13 045. (doi:10.1073/pnas.0905267106)
17. Liegeois R *et al.* 2014 Cerebral functional connectivity periodically (de) synchronizes with anatomical constraints. *Brain Struct. Funct.* (doi:10.1007/s00429-015-1083-y)
18. Hagmann P, Cammoun L, Gigandet X, Meuli R, Honey CJ, Wedeen VJ, Sporns O. 2008 Mapping the structural core of human cerebral cortex. *PLoS Biol.* **6**, e159. (doi:10.1371/journal.pbio.0060159)
19. Hermundstad AM *et al.* 2013 Structural foundations of resting-state and task-based functional connectivity in the human brain. *Proc. Natl Acad. Sci. USA* **110**, 6169–6174. (doi:10.1073/pnas.1219562110)
20. Greicius MD, Supekar K, Menon V, Dougherty RF. 2009 Resting-state functional connectivity reflects structural connectivity in the default mode network. *Cereb. Cortex* **19**, 72–78. (doi:10.1093/cercor/bhn059)
21. Wang Z, Chen LM, Négyessy L, Friedman RM, Mishra A, Gore JC, Roe AW. 2013 The relationship of anatomical and functional connectivity to resting-state connectivity in primate somatosensory cortex. *Neuron* **78**, 1116–1126. (doi:10.1016/j.neuron.2013.04.023)
22. Werner G. 2013 Consciousness related brain processes viewed in the framework of phase space dynamics, criticality, and the renormalization group. *Chaos, Solitons Fract.* **55**, 3–12. (doi:10.1016/j.chaos.2012.03.014)
23. Tagliazucchi E, Fraiman D, Balenzuela P, Chialvo DR. 2012 Criticality in large-scale brain fMRI dynamics unveiled by a novel point process analysis. *Front. Physiol.* **3**, 15. (doi:10.3389/fphys.2012.00015)
24. Werner G. 2007 Metastability, criticality and phase transitions in brain and its models. *Biosystems* **90**, 496–508. (doi:10.1016/j.biosystems.2006.12.001)
25. Kelso JS. 2012 Multistability and metastability: understanding dynamic coordination in the brain. *Phil. Trans. R. Soc. B* **367**, 906–918. (doi:10.1098/rstb.2011.0351)
26. Stam CJ, van Straaten ECW, Van Dellen E, Tewarie P, Gong G, Hillebrand A, Meier J, Van Mieghem P. 2015 The relation between structural and functional connectivity patterns in complex brain networks. *Int. J. Psychophysiol.* (doi:10.1016/j.ijpsycho.2015.02.011)
27. Deco G, McIntosh AR, Shen K, Hutchison RM, Menon RS, Everling S, Hagmann P, Jirsa VK. 2014 Identification of optimal structural connectivity using functional connectivity and neural modeling. *J. Neurosci.* **34**, 7910–7916. (doi:10.1523/JNEUROSCI.4423-13.2014)
28. Massimini M, Ferrarelli F, Huber R, Esser SK, Singh H, Tononi G. 2005 Breakdown of cortical effective connectivity during sleep. *Science* **309**, 2228–2232. (doi:10.1126/science.1117256)
29. Ferrarelli F, Massimini M, Sarasso S, Casali A, Riedner BA, Angelini G, Tononi G, Pearce RA. 2010 Breakdown in cortical effective connectivity during midazolam-induced loss of consciousness. *Proc. Natl Acad. Sci. USA* **107**, 2681–2686. (doi:10.1073/pnas.0913008107)
30. Casali AG *et al.* 2013 A theoretically based index of consciousness independent of sensory processing and behavior. *Sci. Transl. Med.* **5**, 198ra105. (doi:10.1126/scitranslmed.3006294)
31. Pigorini A *et al.* 2015 Bistability breaks-off deterministic responses to intracortical stimulation during non-REM sleep. *NeuroImage*. **112**, 105–113. (doi:10.1016/j.neuroimage.2015.02.056)
32. Solovey G, Alonso LM, Yanagawa T, Fujii N, Magnasco MO, Cecchi GA, Proekt A. 2015 Loss of consciousness is associated with stabilization of cortical activity. *J. Neurosci.* **35**, 10 866–10 877. (doi:10.1523/JNEUROSCI.4895-14.2015)
33. Ramsay MA, Savege TM, Simpson BR, Goodwin R. 1974 Controlled sedation with alphaxalone-alphadolone. *Br. Med. J.* **2**, 656–659. (doi:10.1136/bmj.2.5920.656)
34. Power JD, Mitra A, Laumann TO, Snyder AZ, Schlaggar BL, Petersen SE. 2014 Methods to detect, characterize, and remove motion artifact in resting state fMRI. *Neuroimage* **84**, 320–341. (doi:10.1016/j.neuroimage.2013.08.048)
35. Kantelhardt JW, Koscielny-Bunde E, Rego HH, Havlin S, Bunde A. 2001 Detecting long-range correlations with detrended fluctuation analysis. *Physica A* **295**, 441–454. (doi:10.1016/S0378-4371(01)00144-3)
36. Haimovici A, Tagliazucchi E, Balenzuela P, Chialvo DR. 2013 Brain organization into resting state networks emerges at criticality on a model of the human connectomes. *Phys. Rev. Lett.* **110**, 178101. (doi:10.1103/PhysRevLett.110.178101)
37. Tzourio-Mazoyer N, Landeau N, Papathanassiou B, Crivello D, Etard O, Delcroix N, Mazoyer B, Joliot M. 2002 Automated anatomical labeling of activations in SPM using a macroscopic anatomical parcellation of the MNI MRI single-subject brain. *Neuroimage* **15**, 273–289. (doi:10.1006/nimg.2001.0978)
38. Pigorini A *et al.* 2015 Bistability breaks-off deterministic responses to intracortical stimulation

during non-REM sleep. *Neuroimage* **112**, 105–113. (doi:10.1016/j.neuroimage.2015.02.056)

39. Nir Y, Fisch L, Mukamel R, Gelbard-Sagiv H, Arieli A, Fried I, Malach R. 2007 Coupling between neuronal firing rate, gamma LFP, and BOLD fMRI is related to interneuronal correlations. *Curr. Biol.* **17**, 1275–1285. (doi:10.1016/j.cub.2007.06.066)
40. Tononi G, Sporns O, Edelman GM. 1994 A measure for brain complexity: relating functional segregation and integration in the nervous system. *Proc. Natl Acad. Sci. USA* **91**, 5033–5037. (doi:10.1073/pnas.91.11.5033)
41. Tononi G, Edelman GM. 1998 Consciousness and complexity. *Science* **282**, 1846–1851. (doi:10.1126/science.282.5395.1846)
42. Burgess AP, Rehman J, Williams JD. 2003 Changes in neural complexity during the perception of 3D images using random dot stereograms. *Int. J. Psychophysiol*. **48**, 35–42. (doi:10.1016/S0167-8760(03)00002-3)
43. Dehaene S, Naccache L. 2001 Towards a cognitive neuroscience of consciousness: basic evidence and a workspace framework. *Cognition* **79**, 1–37. (doi:10.1016/S0010-0277(00)00123-2)
44. Priesemann V, Valderrama M, Wibral M, Le Van Quyen M. 2013 Neuronal avalanches differ from wakefulness to deep sleep—evidence from intracranial depth recordings in humans. *PLoS Comput. Biol*. **9**, e1002985. (doi:10.1371/journal.pcbi.1002985)
45. Alonso LM, Proekt A, Schwartz TH, Pryor KO, Cecchi GA, Magnasco MO. 2014 Dynamical criticality during induction of anesthesia in human ECoG recordings. *Front. Neural Circuits* **8**. (doi:10.3389/fncir.2014.00020)
46. Scott G, Fagerholm ED, Mutoh H, Leech R, Sharp DJ, Shew WL, Knöpfel T. 2014 Voltage imaging of waking mouse cortex reveals emergence of critical neuronal dynamics. *J. Neurosci.* **34**, 16 611–16 620. (doi:10.1523/JNEUROSCI.3474-14.2014)
47. Meisel C, Storch A, Hallmeyer-Elgner S, Bullmore E, Gross T. 2012 Failure of adaptive self-organized criticality during epileptic seizure attacks. *PLoS Comput. Biol.* **8**, e1002312. (doi:10.1371/journal.pcbi.1002312)
48. Expert P, Lambiotte R, Chialvo DR, Christensen K, Jensen HJ, Sharp DJ, Turkheimer F. 2010 Self-similar correlation function in brain resting-state functional magnetic resonance imaging. *J. R. Soc. Interface* 20100416. (doi:10.1098/rsif.2010.0416)
49. Barttfeld P, Uhrig L, Sitt JD, Sigman M, Jarraya B, Dehaene S. 2015A Signature of consciousness in the dynamics of resting-state brain activity. *Proc. Natl Acad. Sci. USA* **112**, 887–892. (doi:10.1073/pnas.1418031112)
50. Kaas JH, Gharbawie OA, Stepniewska I. 2013 Cortical networks for ethologically relevant behaviors in primates. *Am. J. Primatol*. **75**, 407–414. (doi:10.1002/ajp.22065)
51. Rilling JK. 2014 Comparative primate neuroimaging: insights into human brain evolution. *Trends Cogn. Sci.* **18**, 46–55. (doi:10.1016/j.tics.2013.09.013)
52. Alkire MTM, Haier RJP, Shah NKM, Anderson CTM. 1997 Positron emission tomography study of regional cerebral metabolism in humans during isoflurane anesthesia. *Anesthesiology* **86**, 549–557. (doi:10.1097/00000542-199703000-00006)
53. Kaisti KK, Metsähonkala L, Teräs M, Oikonen V, Aalto S, Jääskeläinen S, Hinkka S, Scheinin H. 2002 Effects of surgical levels of propofol and sevoflurane anesthesia on cerebral blood flow in healthy subjects studied with positron emission tomography. *Anesthesiology* **96**, 1358–1370. (doi:10.1097/00000542-200206000-00015)
54. Laitio RM *et al.* 2007 Effects of xenon anesthesia on cerebral blood flow in humans: a positron emission tomography study. *Anesthesiology* **106**, 1128–1133. (doi:10.1097/01.anes.0000267596.57497.92)
55. Bonhomme V, Maquet P, Phillips C, Plenevaux A, Hans P, Luxen A, Lamy M, Laureys S. 2008 The effect of clonidine infusion on distribution of regional cerebral blood flow in volunteers. *Anesthesia Analgesia* **106**, 899–909. (doi:10.1213/ane.0b013e3181619685)
56. James W. 1890 *The principles of psychology* (ed. GA Miller). Cambridge, MA: Harvard University Press.
57. Bullmore E, Sporns O. 2009 Complex brain networks: graph theoretical analysis of structural and functional systems. *Nat. Rev. Neurosci*. **10**, 186–198. (doi:10.1038/nrn2575)
58. Fiset P, Plourde G, Backman SB. 2005 Brain imaging in research on anesthetic mechanisms: studies with propofol. *Prog Brain Res* **150**, 245–598. (doi:10.1016/S0079-6123(05)50018-9)
59. Liu X, Pillay S, Li R, Vizuete JA, Pechman KR, Schmainda KM, Hudetz AG. 2013 Multiphasic modification of intrinsic functional connectivity of the rat brain during increasing levels of propofol. *Neuroimage* **83**, 581–592. (doi:10.1016/j.neuroimage.2013.07.003)
60. Veselis RA, Feshchenko VA, Reinsel RA, Beattie B, Akhurst TJ. 2005 Propofol and thiopental do not interfere with regional cerebral blood flow response at sedative concentrations. *Anesthesiology* **102**, 26–34. (doi:10.1097/00000542-200501000-00008)
61. Johnston AJ *et al.* 2003 Effects of propofol on cerebral oxygenation and metabolism after head injury. *Br. J. Anaesth*. **91**, 781–786. (doi:10.1093/bja/aeg256)
62. Hudetz AG, Liu X, Pillay S. 2015 Dynamic repertoire of intrinsic brain states is reduced in propofol-induced unconsciousness. *Brain Connect*. **5**, 10–22. (doi:10.1089/brain.2014.0230)
63. Franceschini MA, Radhakrishnan H, Thakur K, Wu W, Ruvinskaya S, Carp S, Boas DA. 2010 The effect of different anesthetics on neurovascular coupling. *Neuroimage* **51**, 1367–1377. (doi:10.1016/j.neuroimage.2010.03.060)
64. Schröter MS *et al.* 2012 Spatiotemporal reconfiguration of large-scale brain functional networks during propofol-induced loss of consciousness. *J. Neurosci*. **32**, 12 832–12 840. (doi:10.1523/JNEUROSCI.6046-11.2012)
65. Barttfeld P, Bekinschtein TA, Salles A, Stamatakis EA, Adapa R, Menon DK, Sigman M. 2015 Factoring the brain signatures of anesthesia concentration and level of arousal across individuals. *Neuroimage: Clinical* **9**, 385–391. (doi:10.1016/j.nicl.2015.08.013)